

Proton isotropy boundaries as measured on mid- and low-altitude satellites

N. Yu. Ganushkina¹, T. I. Pulkkinen¹, M. V. Kubyschkina², V. A. Sergeev², E. A. Lvova², T. A. Yahnina³, A. G. Yahnin³, and T. Fritz⁴

¹Finnish Meteorological Institute, Space Research Division, FIN-00101 Helsinki, Finland

²Institute of Physics, University of St.-Petersburg, St.-Petersburg, 198904, Russia

³Polar Geophysical Institute, Apatity, Murmansk region, 184200, Russia

⁴Boston University, Department of Astronomy, Boston, MA 02215, USA

Received: 11 September 2004 – Revised: 7 April 2005 – Accepted: 8 April 2005 – Published: 28 July 2005

Abstract. Polar CAMMICE MICS proton pitch angle distributions with energies of 31–80 keV were analyzed to determine the locations where anisotropic pitch angle distributions (perpendicular flux dominating) change to isotropic distributions. We compared the positions of these mid-altitude isotropic distribution boundaries (IDB) for different activity conditions with low-altitude isotropic boundaries (IB) observed by NOAA 12. Although the obtained statistical properties of IDBs were quite similar to those of IBs, a small difference in latitudes, most pronounced on the nightside and dayside, was found. We selected several events during which simultaneous observations in the same local time sector were available from Polar at mid-altitudes, and NOAA or DMSP at low-altitudes. Magnetic field mapping using the Tsyganenko T01 model with the observed solar wind input parameters showed that the low- and mid-altitude isotropization boundaries were closely located, which leads us to suggest that the Polar IDB and low-altitude IBs are related. Furthermore, we introduced a procedure to control the difference between the observed and model magnetic field to reduce the large scatter in the mapping. We showed that the isotropic distribution boundary (IDB) lies in the region where $R_c/\rho \sim 6$, that is at the boundary of the region where the non-adiabatic pitch angle scattering is strong enough. We therefore conclude that the scattering in the large field line curvature regions in the nightside current sheet is the main mechanism producing isotropization for the main portion of proton population in the tail current sheet. This mechanism controls the observed positions of both IB and IDB boundaries. Thus, this tail region can be probed, in its turn, with observations of these isotropy boundaries.

Keywords. Magnetospheric physics (Energetic particles, Precipitating; Magnetospheric configuration and dynamics; Magnetotail)

1 Introduction

Measurements of precipitating energetic protons around the auroral region have been made since the beginning of the space era on board many low-altitude satellites, such as Injun 1 and 3, ESRO IA and IB, NOAA, and DMSP (Søråas, 1972; Imhof et al., 1977; Sergeev et al., 1983; Newell et al., 1998). At each crossing of the auroral zone, there exists a sharp boundary in proton fluxes separating the poleward zone of isotropic precipitation (over the loss cone, i.e. precipitating fluxes are equal to the fluxes of trapped particles with 90° local pitch angles) from the equatorial zone with empty loss cone (fluxes of trapped particles are much higher than precipitating fluxes). This low-altitude boundary at which isotropy is reached in the loss cone is called the isotropic boundary (IB). The characteristic features of the nightside pattern of the energetic particle precipitation can be summarized as follows (Sergeev et al., 1993; Sergeev and Gvozdevsky, 1995): 1) for ions the isotropic boundaries were observed at all MLT and for all activity conditions; 2) the IB latitudes depend on the particle species, energy, MLT and magnetic activity; 3) for ions of the same species and energy, the IB latitude is higher around local noon than at local midnight; 4) for a given species, the higher the energy, the lower the latitude at which the IB is observed. Newell et al. (1998) compared simultaneous observations of IB from NOAA and b2i boundary (latitude of the ion energy flux precipitation peak) from DMSP and showed their close association. Extending this finding Donovan et al. (2003) showed the close relationship of b2i boundary to the equatorward boundary of the proton aurora.

In the equatorial magnetosphere a somewhat similar pattern was observed, in which the proton distributions are isotropic in the plasma sheet (Stiles et al., 1978), which maps to the high-latitude portion of the auroral oval, and become progressively anisotropic towards the dayside. Signatures of isotropization of energetic particle (60–3000 keV) pitch angle distributions were observed in a few cases on

OGO 5 near midnight in the equatorial magnetosphere (West et al., 1978). The AMPTE/CCE spacecraft provided the ion data (1 keV–4 MeV) to study plasma pressure anisotropies at $L < 9$ (Lui and Hamilton, 1992; De Michelis et al., 1999; Milillo et al., 2003). It was shown that the anisotropy $A = (\frac{P_{\perp}}{P_{\parallel}} - 1)100\%$ tends to (1) increase with an L decrease approaching 100% for $L = 3-3.5$, (2) a decrease with increasing activity level and (3) be generally higher in the noon sector than in the midnight sector.

Wave-particle interactions were for a long time considered to be the main mechanism leading to particle precipitation, see, for example, a review by Hultqvist (1979). However, the ability of waves to produce the strong diffusion required to fill the loss cone isotropically is still under question. Also the wave intensity depends on the activity and particle fluxes, which is in contrast to the stable properties of the isotropic precipitation which always requires stable and very high wave activity.

On the other hand, there exists a robust and always operating pitch angle scattering in the magnetic field regions where the conditions for adiabatic particle motion are violated (Alfvén and Fälthammar, 1963; Tsyganenko, 1982; Birmingham, 1984; Büchner and Zelenyi, 1987; Delcourt et al., 1996; Young et al., 2002). In particular, if the effective Larmor radius ($\rho = \frac{mv}{qB}$, where m is the particle mass, v is the total particle velocity, q is the particle charge and B is the magnetic field) becomes comparable to the radius of the field line curvature in the equatorial current sheet ($R_c = \frac{B_z}{\partial B_x / \partial z}$, where B_x and B_z are the magnetic field components), then the first adiabatic invariant is violated and pitch-angle scattering occurs. The ion isotropic boundaries have been shown to be the low-altitude signatures of the boundary between regions of adiabatic and chaotic particle motion in the equatorial magnetosphere (Sergeev et al., 1983). The value of R_c/ρ for the strong scattering depends on the current sheet structure and particle parameters, as well as on the required amplitude of the pitch angle change, but in most conditions it varies between 6 and 10 see e.g. West et al. (1978); Sergeev and Tsyganenko (1982); Delcourt et al. (1996); Young et al. (2002).

Many studies have been done to confirm the action of the pitch angle scattering mechanism for low-altitude isotropic boundaries, both comparing the low-altitude observations of these boundaries and equatorial magnetic field measurements (Sergeev et al., 1983, 1993; Newell et al., 1998) and following the particle trajectories in numerical simulations (Sergeev and Tsyganenko, 1982; Delcourt et al., 1996). At the same time, while observational studies of isotropization of particle distributions in the equatorial magnetosphere and at mid-altitudes have been made (West et al., 1978; Lui and Hamilton, 1992; De Michelis et al., 1999), the corresponding boundaries of distribution isotropization and their formation mechanisms have not been studied in detail. West et al. (1978) considered two cases and showed that the boundary positions agreed with the ones predicted from in-situ magnetic observations. However, it is not possible to assume that

the obtained agreement is valid for other MLTs or activity levels. Moreover, the boundaries observed in the equatorial magnetosphere and at mid-altitudes are probably not the same as low-altitude isotropic boundaries: Their positions depend not only on the scattering processes but also on the magnetospheric convection which creates anisotropies in the particle distributions.

The purpose of this paper is to further explore the relationship between particle scattering in the current sheet and the observed anisotropy characteristics in the mid-altitude magnetosphere. We compare the proton pitch angle distribution isotropization boundary at mid altitudes (measured by Polar CAMMICE/MICS instrument) to the low-altitude isotropic boundaries observed by NOAA satellites during 1997. Several simultaneous conjugate observations at Polar and DMSP or at Polar and NOAA are considered. Using the Tsyganenko T01 model we analyze the statistical distributions of these boundaries mapped into the ionosphere, and evaluate the corresponding R_c/ρ parameters in the equatorial current sheet. Based on these comparisons we conclude that, similar to the low-altitude isotropic boundaries, regular pitch angle scattering in the tail current sheet is the basic mechanism that controls the transition from isotropic to anisotropic distributions in the near-equatorial region.

2 Low- and mid-altitude signatures of pitch-angle isotropization

2.1 NOAA observations of isotropic boundaries (IB)

Figure 1 shows an example of measurements on the MEPED instrument on 1 May 1997 made on board the NOAA 12 spacecraft. The NOAA spacecraft is on a nearly circular, Sun-synchronous polar orbit at an altitude of about 800 km (Hill et al., 1985). The Medium Energy Proton and Electron Detector (MEPED) instrument measures with a time resolution of 2 s the differential flux of protons in the energy range of 30–80 keV. A pair of detectors in the MEPED instrument, one looking radially outward and the other in a perpendicular direction, measure precipitating particles (j_P) in the central part of the loss cone and locally trapped particles outside the loss cone (j_T). Sharp boundaries in proton fluxes separating the poleward isotropic precipitation from the equatorward region with weak filling of the loss cone are marked by vertical lines. Note that in Fig. 1 the precipitating flux exceeds the trapped flux in the isotropy zone. This is a consequence of the fact that the proton detectors suffer radiation damage over time. The impact of this damage is to increase the energy threshold for counting protons, and the increase is stronger for the horizontal detector, as this detector over time has been subjected to the largest radiation dose (see Yahnina et al. (2003) for a brief description of the damage effects).

2.2 Polar CAMMICE/MICS observations of isotropic distribution boundaries (IDB)

The Polar spacecraft was launched in 1995 on an 86° inclination elliptical orbit with a $9 R_E$ apogee, $1.8 R_E$ perigee, and 18-h orbital period. The Charge and Mass Magnetospheric Ion Composition Experiment on board Polar was designed to measure the charge and mass composition of particles within the Earth's magnetosphere over the energy range of 1 keV/Q to 60 MeV/Q (Wilken et al., 1992). The MICS (Magnetospheric Ion Composition Sensor) sensor identifies each ion from measurements of time of flight, energy per charge, and total energy. An electrostatic analyzer allows entry of the ions in one of 32 energy/charge steps in the range of 1–200 keV/e. We analyze the pitch angle distributions of protons with energies of 30–81 keV. In our study we also used magnetic field measurements given by MFE (Magnetic Field Experiment) instrument at Polar which consists of two tri-axial fluxgate magnetometer sensors and measures the vector magnetic field at the spacecraft location (Russell et al., 1995).

Figure 2 presents one example of Polar CAMMICE/MICS measurements on 21 May 1997 at 00:30–02:30 UT (upper panel) in counts per second for pitch angles from zero to 360° . Polar moved inbound from the high-latitude plasma sheet to the ring current region. This gave us a unique opportunity to search for a boundary where the isotropic pitch angle distribution changes to anisotropic at mid-altitudes, between the ionosphere and equatorial plane. Because the resolution in local pitch angle was about 9° , we define the parallel (to the magnetic field) count rate as a sum of counts for wide sectors of pitch angles from 0° to 45° and the perpendicular count rate as a sum of counts for pitch angles from 45° to 90° at a given UT. They are shown in the middle panel of the Fig. 2 by thick and thin lines, respectively. The bottom panel shows the ratio between the parallel and perpendicular count rates. For each pair, we determine the first point at which the ratio between the parallel and perpendicular count rates is within 0.8 and 1.2 (two horizontal lines) tailward of the maximum of the perpendicular count rate. We call this point the isotropic distribution boundary (IDB). This point is marked by a vertical line in all three panels, and it shows that the isotropization of the pitch angle distribution occurred at 00:50 UT, 21:50 MLT, $L=7.7$, R (radial distance) = $4.6 R_E$ and latitude of the spacecraft was 39.5° . The corresponding value of total magnetic field was about 400 nT.

2.3 Statistical results

We analyzed one year (1997) of Polar measurements, when the orbit apogee was over the northern polar region. Figure 3 shows the corrected geomagnetic latitudes of the IDBs (red crosses) as a function of MLT for three ranges of the D_{St} index: a) $-10 \text{ nT} < D_{St} < 10 \text{ nT}$, b) $-50 \text{ nT} < D_{St} < -10 \text{ nT}$, and c) $D_{St} < -50 \text{ nT}$. The corrected geomagnetic latitudes of the IDBs were determined using a mapping with the Tsyganenko T01 magnetospheric magnetic field model (Tsyga-

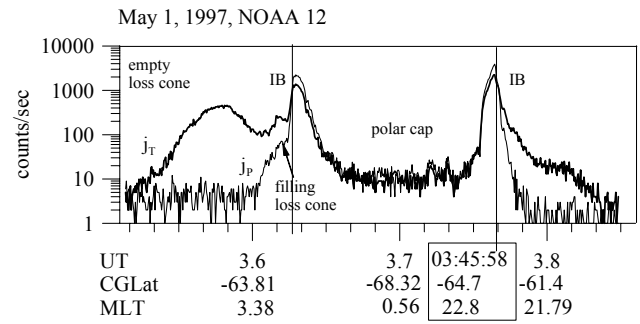


Fig. 1. Example of NOAA 12 measurements on 1 May 1997 showing the sharp boundaries marked by vertical lines when precipitating particle fluxes (j_P) in the central part of the loss cone and locally trapped particle fluxes outside the loss cone (j_T) become comparable.

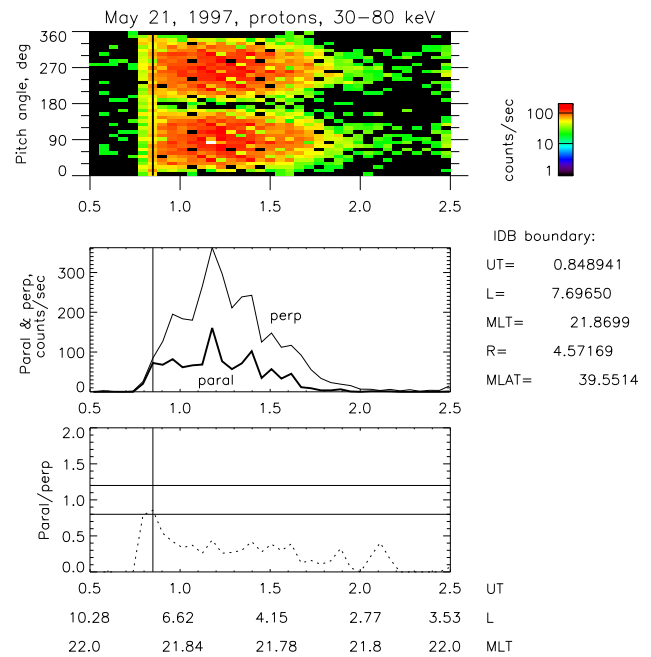


Fig. 2. (top panel) Polar CAMMICE/MICS measurements of proton pitch angle distributions in the energy range of 31–80 keV, (middle panel) parallel (thick line) and perpendicular (thin line) count rates, and (bottom panel) the ratio between the parallel and perpendicular count rates for 21 May 1997, 00:30–02:30 UT. The position of IDB is marked by a vertical line at all three panels.

nenko, 2002a,b). The input parameters for each IDB observation, interplanetary magnetic field and solar wind dynamic pressure, were obtained from the WIND spacecraft. Figure 3 also presents the statistical positions of isotropic boundaries for protons with an energy range of 30–80 keV observed on the NOAA 12 satellite during 1997 in the Northern (open triangles) and Southern (open circles) Hemispheres. Latitudes of the isotropic boundaries (IB) in the Southern Hemisphere are plotted as absolute values. As can be seen, the IB positions in Southern and Northern Hemispheres do not differ significantly. Plotting both hemispheres was used to increase the statistics of the IB positions.

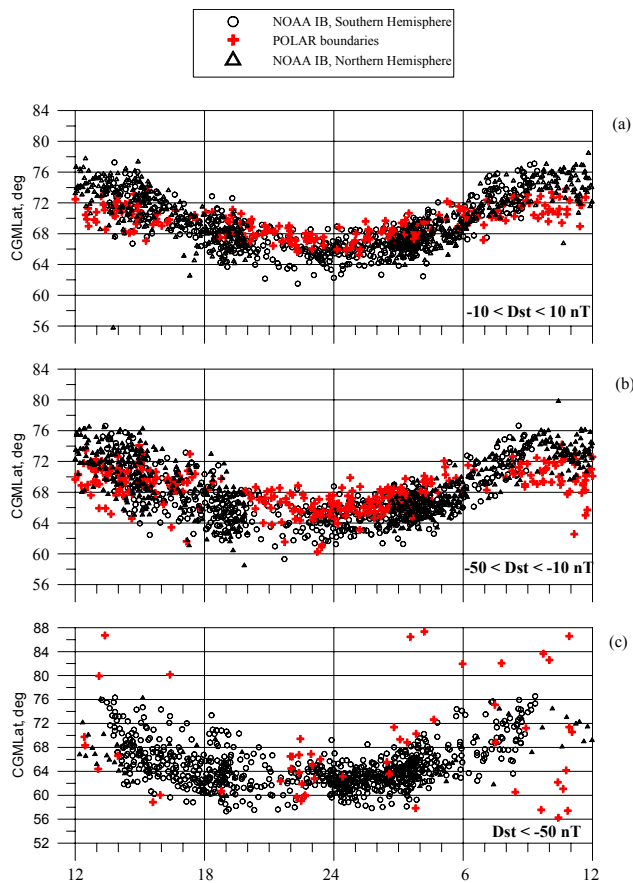


Fig. 3. MLT-dependence of corrected geomagnetic latitudes of isotropic distribution boundaries (IDB) observed by Polar CAMMICE/MICS (red crosses), together with isotropic boundaries (IB) observed by NOAA 12 satellites in the Northern (open triangles) and Southern (open circles) Hemispheres for (a) $-10 \text{ nT} < D_{st} < 10 \text{ nT}$, (b) $-50 \text{ nT} < D_{st} < -10 \text{ nT}$, and (c) $D_{st} < -50 \text{ nT}$.

The obtained statistical properties of IDBs are quite similar to those of the IBs (Sergeev and Gvozdevsky, 1995). These boundaries (IDBs and IBs) were observed at all MLTs. There exists a day-night asymmetry with the night-side boundaries being at lower latitudes than those on the dayside. An increase of activity (decrease in the D_{st} index) leads to an equatorward shift of boundaries at all MLTs. At the same time, there exists a small difference between average IDB and IB latitudes which is most pronounced on the nightside and on the dayside. For the quiet conditions with $-10 \text{ nT} < D_{st} < 10 \text{ nT}$ IDBs are observed in the latitudinal range of 65° – 69° on the nightside and 69° – 73° on the dayside. IDBs are observed below 64° (60°) on the nightside and 68° (65°) on the dayside for $-50 \text{ nT} < D_{st} < -10 \text{ nT}$ ($D_{st} < -50 \text{ nT}$). The IDB positions become more scattered and occupy a larger latitudinal interval at a given MLT than the IBs. A very scattered pattern is observed during disturbed conditions when $D_{st} < -50 \text{ nT}$. For all three D_{st} ranges IBs are observed at lower latitudes than IDBs on the nightside.

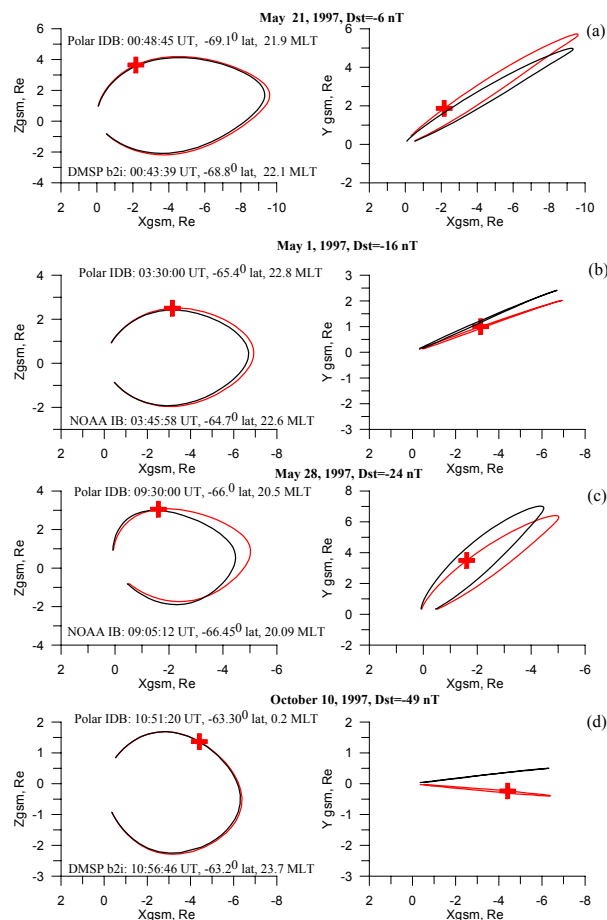


Fig. 4. Noon-midnight meridian (left panels) and equatorial plane (right panels) projections of the magnetic field lines corresponding to DMSP or NOAA (black lines) and Polar (red line) locations, when the conjugate boundaries were observed at Polar and DMSP on (a) 21 May 1997 and (d) 10 October 1997, and at Polar and NOAA on (b) 1 May 1997 and (c) 28 May 1997. The thick red cross shows the Polar location.

3 Comparison of mid-altitude and low-altitude conjugate observations

In addition to the comparison of statistical results on mid-altitude IDBs as observed by Polar and low-altitude IBs observed by NOAA, we searched for several conjugate observations by Polar and NOAA, and Polar and DMSP. Like the NOAA spacecraft, the DMSP satellites have a 101-min Sun-synchronous, near-polar orbit at 830 km altitude. Using the observations made in 1997, for both Polar and NOAA, and Polar and DMSP, we searched for cases when NOAA and DMSP observations and Polar observations were within 30 min of each other ($\Delta \text{UT} < 30 \text{ min}$) and in the same local time sector ($\Delta \text{MLT} < 30 \text{ min}$). For Polar and DMSP conjunctions, we used IDBs at Polar and the b2i boundary (the energetic ion precipitation flux peak) at DMSP which corresponds well to the proton isotropic precipitating boundary at 30 keV energy (Newell et al., 1998).

Table 1. Positions of Polar, NOAA and DMSP satellites for conjugate events, together with solar wind parameters, D_{st} index, and corresponding magnetic field line parameters.

Satellite	UT	MLT	CGMlat, °	R_{eq}, R_E	CGMlat model, °
21 May 1997					
$(P_{sw}=0.8 \text{ nPa}, D_{st}=-6 \text{ nT}, \text{IMF } B_y=0.4 \text{ nT}, \text{IMF } B_z=1.8 \text{ nT})$					
Polar	00:48	21:54	69.1	11.2	68.04
DMSP	00:43	22:06	68.8	10.6	67.94
Δ	5 min	12 min	0.3°	0.6 R_E	0.1°
1 May 1997					
$(P_{sw}=3.1 \text{ nPa}, D_{st}=-16 \text{ nT}, \text{IMF } B_y=-2.6 \text{ nT}, \text{IMF } B_z=-1.3 \text{ nT})$					
Polar	03:30	22:48	65.4	7.2	65.06
NOAA	03:46	22:36	64.7	7.1	65.47
Δ	16 min	12 min	0.7°	0.1 R_E	0.41°
28 May 1997					
$(P_{sw}=2.8 \text{ nPa}, D_{st}=-24 \text{ nT}, \text{IMF } B_y=-0.4 \text{ nT}, \text{IMF } B_z=0.6 \text{ nT})$					
Polar	09:30	20:30	66.9	8.3	66.54
NOAA	09:05	20:05	66.45	8.1	66.92
Δ	25 min	25 min	0.45°	0.2 R_E	0.38°
10 October 1997					
$(P_{sw}=2 \text{ nPa}, D_{st}=-49 \text{ nT}, \text{IMF } B_y=2 \text{ nT}, \text{IMF } B_z=-3.8 \text{ nT})$					
Polar	10:51	00:12	63.3	6.4	63.91
DMSP	10:57	23:42	63.2	6.3	63.89
Δ	6 min	25 min	0.1°	0.1 R_E	0.02°

Figure 4 presents two selected conjunctions between Polar and DMSP for a) 21 May 1997 and d) 10 October 1997, and two between Polar and NOAA for b) 1 May 1997 and c) 28 May 1997. These cases were selected to cover the interval of activity conditions from quiet with $D_{st}=-6 \text{ nT}$ on 21 May 1997, to disturbed with $D_{st}=-49 \text{ nT}$ on 10 October 1997. Noon-midnight meridian (left panels) and equatorial plane (right panels) projections of the magnetic field lines corresponding to DMSP or NOAA (black lines) and Polar (red line) locations, when the isotropy boundaries were observed, are shown. We used the Tsyganenko T01 model (Tsyganenko, 2002a,b) with the observed solar wind conditions and D_{st} index as input parameters for the magnetic field calculations. The thick red cross shows the Polar location.

Table 1 presents, together with corresponding IMF and solar wind parameters and D_{st} indices, the UTs and MLTs of the positions of IDBs, IBs and b2i boundaries observed by Polar, NOAA and DMSP, respectively. The corrected geomagnetic latitudes and equatorial distances for corresponding magnetic field lines calculated using the Tsyganenko T01 model with the observed parameters for the four selected conjugate events are also shown.

For all four cases, independent of the activity conditions, the differences in latitudes of the observed IDBs at Polar and IB at NOAA and b2i at DMSP were rather small, less than 1°, with a maximum difference of 0.7° on 1 May 1997, when D_{st} was equal to -16 nT . The difference in equatorial radial distance was also small, reaching 0.6 R_E on 21 May 1997, when D_{st} was about -6 nT .

We also computed the model locations of the expected isotropy boundaries by finding the magnetic field lines (at MLTs of Polar, NOAA and DMSP) on which the criterion of $R_c/\rho=8$ is fulfilled (Sergeev and Tsyganenko, 1982). For Polar data we are restricted by 9° in pitch angle and an 8-energy level resolution for the count rates. This seriously limits our possibility to gain information about the detailed structure of the distribution function in this rather limited energy range of 30–80 keV. In our model calculations we used the proton energy of 30 keV. We assumed that the distribution is close to Maxwellian and thus the maximum will be for lower energies. The larmor radius for low energy particles will be smaller, and hence the ratio R_c/ρ will be larger. Making calculations for the energy of 30 keV, we find the maximum R_c/ρ values for the given energy range of 30–80 keV.

The latitudes of model and observed boundaries, shown in the last column in Table 1, are quite close to each other. The differences in latitudes between the model boundaries for conjugate Polar, NOAA and DMSP observations are also small, not exceeding 0.4°.

4 Discussion

We determined the locations of mid-altitude isotropic distribution boundaries (IDB), where anisotropic pitch angle distributions (perpendicular flux dominating) change to isotropic distributions using Polar CAMMICE MICS proton data and compared them to the low-altitude isotropic bound-

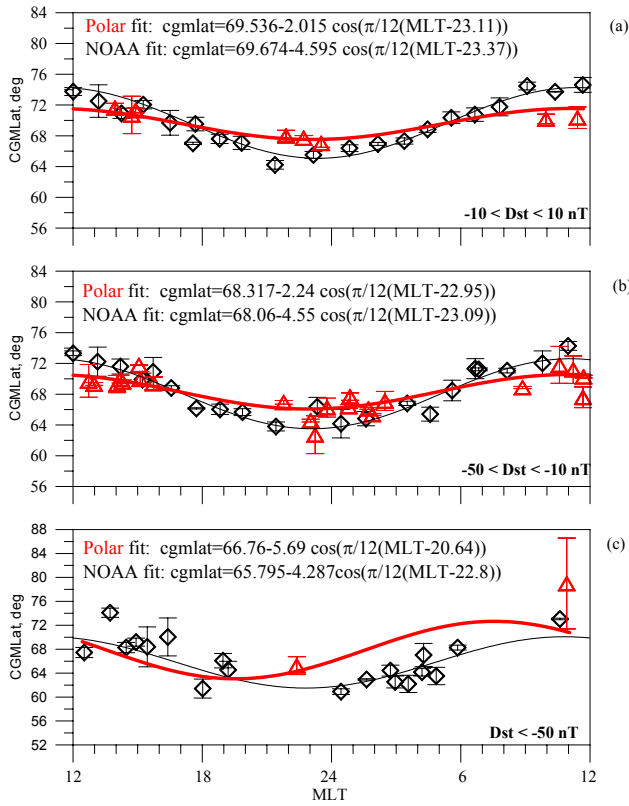


Fig. 5. $Lat(MLT)=A_0-A_1\cos(\pi(MLT-MLT_0)/12)$ approximation for Polar IDB statistics (red curves) and NOAA IB statistics (black curves) (a) $-10\text{ nT}<D_{st}<10\text{ nT}$, (b) $-50\text{ nT}<D_{st}<-10\text{ nT}$, and (c) $D_{st}<-50\text{ nT}$. Standard error means are shown by open red triangles for Polar data and by open black diamonds for NOAA data.

aries (IB) observed by NOAA and DMSP satellites during 1997. The fact that the mid-altitude IDB and low-altitude IB and b2i boundaries were found on very close field lines (Fig. 4) suggests that they are associated with the same isotropization mechanism. Simultaneous observations of isotropization signatures at low- and mid-altitudes is a strong argument supporting the mechanism of filling the ionospheric loss cone by pitch angle scattering due to violation of first adiabatic invariant while crossing the tail current sheet.

Statistical CGLat-MLT dependencies of the IDB and IB positions were found to be very similar, but systematic differences in their latitudes exist most pronounced on the nightside and on the dayside (Fig. 3). Following Sergeev and Gvozdevsky (1995) we fitted the statistical observations by Polar and NOAA using a simple cosine approximation $Lat(MLT)=A_0-A_1\cos(\pi(MLT-MLT_0)/12)$, where A_0 is the average latitude, A_1 is the amplitude and MLT_0 is the phase shift. Figure 5 shows the fits for Polar IDB statistics (red curves) and NOAA IB statistics (black curves) for (a) $-10\text{ nT}<D_{st}<10\text{ nT}$, (b) $-50\text{ nT}<D_{st}<-10\text{ nT}$, and (c) $D_{st}<-50\text{ nT}$. Standard error means are shown by open red triangles for Polar and by open black diamonds for NOAA.

For all three cases IDBs are observed at higher latitudes on the nightside and at lower latitudes on the dayside than IBs. The phase shift towards the dusk exists for both boundaries (increasing with the activity increase) and is larger for Polar IDBs than for NOAA IBs, similar to that previously reported for isotropic and b2i boundaries (Newell et al., 1998) and proton auroras (Donovan et al., 2003). The sparse MLT coverage, however, does not allow for a more detailed investigation of this feature in our data set.

Although we compared directly the locations of IBs observed by low-altitude NOAA satellite and IDBs observed by mid-altitude Polar satellite, it should be clearly mentioned that these two boundaries have a different definition. Low-altitude NOAA MEPED detectors look radially outward and perpendicular to the satellite velocity vector and measure only precipitating and locally mirroring particles. In these data, particles seen in the two directions have very small pitch angle separation at the equator: particles with 10° and 80° pitch angles detected by NOAA will have only 0.31° and 1.78° pitch angles at the equator ($\sim 9 R_E$). The low-altitude isotropic boundary (IB) reflects the transition from the empty loss cone to the isotropically filled loss cone, therefore, it characterizes the pitch angle change during one traversal of the equatorial current sheet. However, the required pitch angle change is very small, of the order of the loss-cone size in the current sheet center, i.e. about $1-2^\circ$.

We define the IDB at Polar not in terms of filling the loss cone but as a boundary where the parallel count rate (sum of counts for pitch angles from 0° to 45°) and the perpendicular count rate (sum of counts for pitch angles from 45° to 90°) become comparable (Fig. 2). Polar IDB is observed at mid-altitudes (total magnetic field is about 300–400 nT), where a large portion of the equatorial plasma distribution is present. IDB characterizes a change in the entire distribution, rather than a change in a small part near the small loss cone like the IB. This change is formed by the interaction of two competitive processes. One of them is pitch angle scattering due to the non-adiabatic motion, which isotropizes the distribution. The other process is the inward convection in the inner magnetosphere, which creates a pancake-like anisotropy due to the dominating betatron acceleration. For that reason, one would expect the IDB at larger distances than the IB on the nightside, where the pitch angle scattering is presumably stronger, which was indeed the case.

To have an idea where in the magnetosphere pitch angle scattering can occur, we integrated particle trajectories with a standard method of 4th order Runge-Kutta scheme in the T01 magnetic field model with quiet-time parameters. Figure 6 illustrates the results for protons with 30 keV. It shows the R_c/ρ -dependence of the phase-averaged pitch angle changes after one crossing of the field reversal region at the midnight meridian. Each point is the average of 18 trajectories, which differ by initial phase. Initial pitch angles varied from 0° to 35° (with 5° step), whereas the initial phase for each initial pitch angle varied from 0° to 360° (in 20° steps). The pitch angles are reduced to the equator.

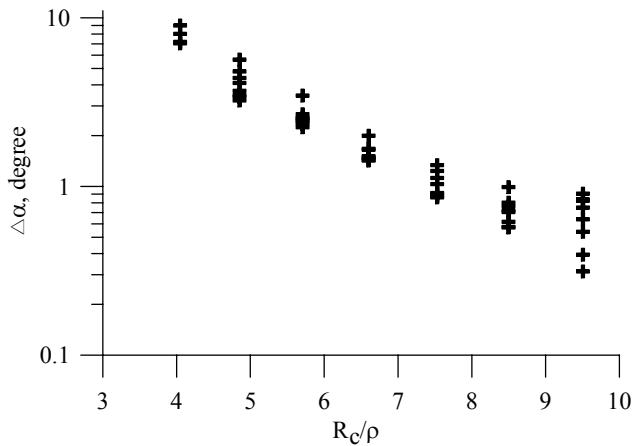


Fig. 6. R_c/ρ -dependence of the phase-averaged pitch angle changes (pitch angles reduced to the magnetic equator) after one crossing of the field reversal region calculated by tracing the 30-keV protons in the T01 magnetic field at midnight meridian. Initial pitch angles varied from 0° to 35° (with 5° step), whereas the initial phase for each initial pitch angle varied from 0° to 360° (in 20° steps).

Similar to previous computations (Sergeev and Tsyganenko, 1982; Delcourt et al., 1996), the pitch angle change is small for large $R_c/\rho \geq 10$ (of the order of the loss-cone size $\sim 0.7^\circ$, when $R_c/\rho \sim 8$) and strongly increases with further decreasing of R_c/ρ . When R_c/ρ falls below 5–6, the scattering increases by a factor of 2.5 and it quickly isotropizes the distribution. This is the location where the IDB is expected to be observed on the nightside. The statistical observations of IDBs at higher latitudes than IBs on the nightside qualitatively agree with this picture.

Having computed the T01 model for each Polar observation point, we mapped the observed IDB locations to the equatorial plane in order to check the R_c/ρ values. As shown in Fig. 4, using the criterion $R_c/\rho = 8$ to determine the latitudes of isotropy boundaries predicted by the magnetic field model the results differed from the observed ones by about $1\text{--}2^\circ$. An obvious reason for that is the error in the model magnetic field, which may be evaluated by comparison with the observed magnetic field value.

The position of the modelled IDB can be influenced by the choice of the energy for which the calculations of R_c/ρ are made, the value of R_c/ρ itself, which is selected as a criteria for the pitch angle scattering and the accuracy of the magnetic field model. We can estimate the differences coming from energy or R_c/ρ changing. As simple calculations have shown, for 10 October 1997 event (Fig. 4d) for protons with 30 keV energy the model IDB latitude is 63.9° for $R_c/\rho = 8$ and 64.16° for $R_c/\rho = 6$. For protons with 80 keV energy the latitude is equal to 63.44° $R_c/\rho = 8$. Thus, changing the energy or R_c/ρ value does not produce big changes in the model IDBs and does not influence our conclusions. It is more difficult to estimate properly the error coming from the magnetic field model. When we have a good correspondence

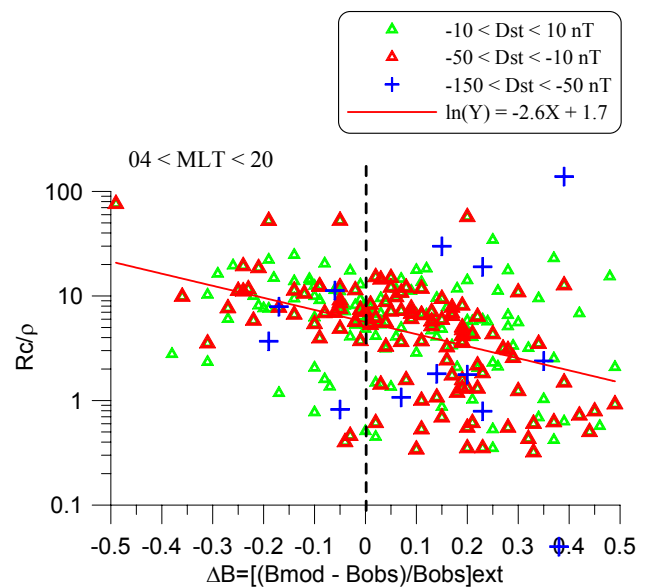


Fig. 7. Dependence of the computed values of R_c/ρ on the accuracy parameter $\Delta B = \frac{B_{T01} - B_{obs}}{B_{obs}}$ corresponding to the Polar IDB observations on the nightside ($04 < MLT < 20$) for $-10 \text{ nT} < D_{st} < 10 \text{ nT}$ (green triangles), $-50 \text{ nT} < D_{st} < -10 \text{ nT}$ (red triangles) and $-150 \text{ nT} < D_{st} < -50 \text{ nT}$ (blue crosses). Here the interval of ΔB from -0.5 to 0.5 is shown as it represents good accuracy. The red line represents the fit $\ln(R_c/\rho) = -2.6 \Delta B + 1.7$.

between the observed and modelled magnetic field at the Polar location, we do not know if the model is accurate at the equator where we estimate the field line curvature. For this, the close location of the magnetic field lines corresponding to observations of IDB on Polar, IB on NOAA, and b2i on DMSP, is an indicator of the model's sufficient accuracy.

To check further the accuracy of the magnetic field model used in the present study, for each Polar observation of IDB on the nightside ($04 < MLT < 20$) we computed a relative error parameter $\Delta B = \frac{B_{T01} - B_{obs}}{B_{obs}}$, where B_{T01} is the external magnetic field calculated using the Tsyganenko T01 model with the observed parameters and B_{obs} is the observed external magnetic field (internal magnetic field given by IGRF model was subtracted from the observed magnetic field) given by the Polar MFE instrument. Then, for each Polar position we computed the value of R_c/ρ using the T01 model, assuming the proton energy to be 30 keV. Figure 7 shows the dependence of the computed values of R_c/ρ on the accuracy parameter ΔB corresponding to the Polar IDB observations for $-10 \text{ nT} < D_{st} < 10 \text{ nT}$ (green triangles), $-50 \text{ nT} < D_{st} < -10 \text{ nT}$ (red triangles) and $-150 \text{ nT} < D_{st} < -50 \text{ nT}$ (blue crosses). Here we show the interval of ΔB from -0.5 to 0.5 . It can be seen that for all D_{st} ranges the computed R_c/ρ increases with ΔB decrease. When $\Delta B < 0$, then $B_{T01} < B_{obs}$. This means that the model underestimates the tail currents, and the model magnetic field line is less stretched than the observed one. The model R_c/ρ value is larger than needed for scattering, and scattering occurs further tailward. When $\Delta B > 0$, then $B_{T01} > B_{obs}$, and

the model magnetic field lines are too stretched. The scattering occurs at larger R_c/ρ values than given by the model.

In Fig. 7 the red line represents the fit $\ln(R_c/\rho) = -2.6 \Delta B + 1.7$. The scattering criterion is determined at the intersection of this fit, and is about 6, and $\Delta B = 0$. The obtained value of R_c/ρ agrees well with our expectations based on the strength of pitch angle scattering and confirms that the regular mechanism of non-adiabatic particle scattering in the current sheet is responsible for maintaining the isotropic proton distribution functions on the nightside. It also supports the conclusions made by West et al. (1978) from two in-situ comparisons of theoretical and observed boundaries. Taking into account the consistency between IDB and IB boundary locations at dusk and dawn (where convection lines go along the boundary and where convection plays a minor role in the restoring the anisotropy), one may also expand this conclusion to the dusk and dawn portions of the IDB distribution.

On the other hand, according to Fig. 6, at $R_c/\rho = 6$ the changes in the particle pitch angle can be as large as several degrees, which confirms our speculations concerning the requirement of stronger scattering for producing IDBs seen at Polar. It is also necessary to mention that the magnetospheric magnetic field models used for magnetic field mapping usually overestimate the thickness of the tail current sheet, which can lead to even smaller values of R_c/ρ than 6.

As was mentioned above, calculations were made for the energy of 30 keV, assuming the distribution to be close to Maxwellian with a maximum at lower energies. The changing in the energy from the lower limit of the energy range (30 keV) to the upper limit (80 keV) will result in the shift of the corresponding fit (Fig. 7), and a lower intersection of this fit and $\Delta B = 0$, to lower R_c/ρ values, but will not lead to a dramatic change in the expected trend for IDB points and our conclusions.

Although we discussed only the nightside isotropic distribution boundaries, we may expect the same physics to be valid for the dayside boundaries. However, it is more difficult to obtain experimental confirmation and to control the mapping errors in that region. The field lines here experience strong 3-D deformations: two field lines which are close by may map to very different domains in the equatorial plane. For example, the field line coming from near the cusp can map to either near the dayside magnetopause (where the magnetic field is strong and R_c/ρ is very large) or to near the magnetopause in the far magnetotail (where the magnetic field and R_c/ρ are very small). Also, these deformations are very sensitive to the intensity and distribution of the field-aligned currents. In general, this region is described with less confidence in the magnetospheric models. This does not allow us to interpret the dayside observations in the same way as we did for the nightside.

When finding the IDBs observed by Polar, we considered only local measurements, not following the pitch-angle distribution evolution and not mapping to the equatorial plane. Also a comparison with DMSP was made using local measurements. At the same time, the particles drift so that the measured distributions at Polar and DMSP may be differ-

ent. Tracing of particle trajectories in realistic magnetic field models and comparison with pitch angle observations is our future task.

The isotropization of the distribution at Polar does not necessarily mean isotropic precipitation of ions at low-altitudes at the same time; other local mechanisms of isotropization at Polar altitudes could well be active. The role of wave-particle interactions in the process of isotropization at different altitudes needs to be investigated further in a future study.

5 Conclusions

In this paper we confirm and extend previous results describing and explaining the transition from anisotropic proton distributions in the near-Earth tail to the isotropic distributions in the nightside plasma sheet.

We showed that two different boundaries (IB, related to the isotropic filling of the loss cone by non-adiabatic pitch angle scattering, and IDB, characterizing the pitch angle distributions in the near-equatorial magnetosphere) stay on the neighboring field lines and display similar CGLatitude-MLT distributions and similar activity dependence. Furthermore, introducing a procedure to control the difference between observed and the model magnetic field we were able to reduce a large scatter in mapped equatorial parameters and to conclude that the isotropic distribution boundary (IDB) lies in the region where $R_c/\rho \sim 6$. In this region the pitch angle scattering is strong enough ($> 10^\circ$ for one current sheet crossing by a test particle). We, therefore, conclude that the scattering in the large field-line curvature regions of the nightside current sheet is the main mechanism producing isotropization for the main portion of proton population in the tail current sheet. This mechanism controls the observed positions of the IB and IDB boundaries and, therefore, can be probed with observations of these isotropy boundaries.

Acknowledgements. We would like to thank K. Ogilvie and R. Leping for the use of WIND data, C. Russell for Polar MFE data obtained from the Coordinated Data Analysis Web (CDAWeb) and World Data Center C2 for Geomagnetism, Kyoto, for the provisional D_{st} indices data. We thank P. Newell for the DMSP b2i boundaries available from JHU/APL website. The NOAA data were obtained from WDC for Aurora, NIPR, Tokyo, Japan. This work was supported by Academy of Finland. The work of M. Kubyskhina, V. Sergeev and E. Lvova was supported by RFBR grant 04-05-64932. The work of T. Yahnina and A. Yahnin was supported by the Division of Physical Sciences of Russian Academy of Science via the program DPS-18.

Topical Editor in chief thanks L. Zelenyi and F. Söraas for their help in evaluating this paper.

References

- Alfvén, H. and Fälthammar, C. G.: *Cosmic Electrodynamics, Fundamental Principles*, (2nd edition), Clarendon, Oxford, 1963.
- Ashour-Abdalla, M. and Kennel, C. F.: Diffuse auroral precipitation, *J. Geomagn. Geoelectr.*, 30, 239–255, 1978.

- Birmingham, T. J.: Pitch angle diffusion in the Jovian magnetodisc, *J. Geophys. Res.*, 89, 2699–2707, 1984.
- Büchner, J. and Zelenyi, L. M.: Chaotization of the electron motion as the cause of an internal magnetotail instability and substorm onset, *J. Geophys. Res.*, 92, 13 456–13 466, 1987.
- Delcourt, D. C., Sauvaud, J.-A., Martin, Jr., R. F. and Moore, T. E.: On the nonadiabatic precipitation of ions from the near-earth plasma sheet, *J. Geophys. Res.*, 101, 17 409–17 418, 1996.
- De Michelis, P., Daglis, I. A., and Consolini, G.: An average image of proton plasma pressure and of current systems in the equatorial plane derived from AMPTE/CCE-CHEM measurements, *J. Geophys. Res.*, 104, 28 615–28 624, 1999.
- Donovan, E. F., Jackel, B. J., and Voronkov, I., et al.: Ground-based optical determination of the b2i boundary: A basis for an optical MT-index, *J. Geophys. Res.*, 108, SMP 10-1, CiteID 1115, doi:10.1029/2001JA009198, 2003.
- Hill, V. D., Evans, D. S. and Sauer, H. H.: TIROS/NOAA satellites space environment monitor, Archive tape documentation, NOAA Tech. Mem. ERL SEL-71, 50, Environ. Res. Lab., Boulder, 1985.
- Hultqvist, B.: The hot ion component of the magnetospheric plasma and some relations to the electron component: Observations and physical implications, *Space Sci. Rev.*, 23, 581–675, 1979.
- Imhof, W. L., Reagan, J. B. and Gaines, E. E.: Fine-scale spatial in the pitch angle distributions of energetic particles near the midnight trapping boundary, *J. Geophys. Res.*, 82, 5215–5221, 1977.
- Imhof, W. L., Reagan, J. B., and Gaines, E. E.: Studies of the sharply defined L dependent energy threshold for isotropy at the midnight trapping boundary, *J. Geophys. Res.*, 84, 6371–6384, 1979.
- Lui, A. T. Y. and Hamilton, D. C.: Radial profiles of quiet time magnetospheric parameters, *J. Geophys. Res.*, 97, 19 325–19 332, 1992.
- Milillo, A., Orsini, S., Delcourt, D. C., et al.: Empirical model of proton fluxes in the equatorial inner magnetosphere: 2. Properties and applications, *J. Geophys. Res.*, 108, 1165, doi:10.1029/2002JA009581, 2003.
- Newell, P. T., Sergeev, V. A., Bikkuzina, G. R. and Wing, S.: Characterizing the state of the magnetosphere: Testing the ion precipitation maxima latitude (b2i) and the ion isotropy boundary, *J. Geophys. Res.*, 103, 4739–4745, 1998.
- Russell, C. T., Snare, R. C., Means, J. D., et al.: The GGS/Polar Magnetic Fields Investigation, *Space Sci. Rev.*, 71, 563–582, 1995.
- Sergeev, V. A. and Gvozdevsky, B. B.: MT-index – A possible new index to characterize the magnetic configuration of magnetotail, *Ann. Geophys.*, 13, 1093–1103, 1995, **SRef-ID: 1432-0576/ag/1995-13-1093**.
- Sergeev, V. A., Malkov, M., and Mursula, K.: Testing the isotropic boundary algorithm method to evaluate the magnetic field configuration in the tail, *J. Geophys. Res.*, 98, 7609–7620, 1993.
- Sergeev, V. A., Sazhina, E. M., Tsyganenko, N. A., Lundblad, J. A., and Soraas, F.: Pitch-angle scattering of energetic protons in the magnetotail current sheet as the dominant source of their isotropic precipitation into the nightside ionosphere, *Planet. Space Sci.*, 31, 1147–1155, 1983.
- Sergeev, V. A. and Tsyganenko, N. A.: Energetic particle losses and trapping boundaries as deduced from calculations with a realistic magnetic field model, *Planet. Space Sci.*, 30, 999–1006, 1982.
- Stiles, G. S., Hones, Jr., E. W., Bame, S. J., and Asbridge, J. R.: Plasma sheet pressure anisotropies, *J. Geophys. Res.*, 83, 3166–3172, 1978.
- Søraas, F.: ESRO IA/B observations at high latitudes of trapped and precipitating protons with energies above 100 keV, in: Earths magnetospheric processes, edited by: B. M. McCormac, 121–132, D. Reidel, Norwell, Mass., 1972.
- Taylor, H. E. and Hastie, R. J.: Nonadiabatic behavior of radiation belt particles, *Cosmic Electrodyn.*, 2, 211–223, 1971.
- Tsyganenko, N. A.: Pitch-angle scattering of energetic particle in the current sheet of the magnetospheric tail and stationary distribution functions, *Planet. Space Sci.*, 30, 433–437, 1982.
- Tsyganenko, N. A.: A model of the near magnetosphere with a dawn-dusk asymmetry: 1. Mathematical structure, *J. Geophys. Res.*, 107, SMP 12-1, CiteID 1179, doi:10.1029/2001JA0002192001, 2002a.
- Tsyganenko, N. A.: A model of the near magnetosphere with a dawn-dusk asymmetry: 2. Parameterization and fitting to observations, *J. Geophys. Res.*, 107, SMP 10-1, CiteID 1176, doi:10.1029/2001JA000220, 2002b.
- Wagner, J. S., Kan, J. R., and Akasofu, S.-I.: Particle dynamics in the plasma sheet, *J. Geophys. Res.*, 84, 891–897, 1979.
- West, H. I., Jr., Buck, R. M., and Kivelson, M. G.: On the configuration of the magnetotail near midnight during quiet and weakly disturbed periods: State of the magnetosphere, *J. Geophys. Res.*, 83, 3805–3817, 1978.
- Wilken, B., Weiss, W., Hall, D., Grande, M., Soraas, F., and Fennell, J. F.: Magnetospheric ion composition spectrometer on board the CRRES spacecraft, *J. Spacecr. Rockets*, 29, 585–591, 1992.
- Yahnina T. A., Yahnin, A. G., Kangas, J., et al.: Energetic particle counterparts for geomagnetic pulsations of Pc1 and IPDP types, *Ann. Geophys.*, 21, 2281–2292, 2003, **SRef-ID: 1432-0576/ag/2003-21-2281**.
- Young, S. L., Denton, R. E., Anderson, B. J., and Hudson, M. K.: Empirical model for μ scattering caused by field line curvature in a realistic magnetosphere, *J. Geophys. Res.*, 107, 1069, doi:10.1029/2000JA000294, 2002.